*Limnol. Oceanogr.*, 42(8), 1997, 1660–1672


# Impact of cell shape and chain formation on nutrient acquisition by marine diatoms

*Markus Pahlow, Ulf Riebesell, and Dieter A. Wolf-Gladrow*
Alfred-Wegener-Institut für Polar- und Meeresforschung, P.O. Box 120161, D-27515 Bremerhaven, Germany

*Abstract*

Diatoms have evolved a multitude of morphologies, including highly elongated cells and cell chains. Elongation and chain formation have many possible functions, such as grazing protection or effects on sinking. Here, a model of diffusive and advective nutrient transport is used to predict impacts of cell shape and chain length on potential nutrient supply and uptake in a turbulent environment. Rigid, contiguous, prolate spheroids thereby represent the shapes of simple chains and solitary cells. At scales larger than a few centimeters, turbulent water motions produce a more or less homogeneous nutrient distribution. At the much smaller scale of diatom cells, however, turbulence creates a roughly linear shear and nutrients can locally become strongly depleted because of nutrient uptake by phytoplankton cells. The potential diffusive nutrient supply is greater for elongated than for spherically shaped cells of similar volume but lower for chains than for solitary cells. Although the relative increase in nutrient transport due to turbulence is greater for chains, single cells still enjoy a greater total nutrient supply in turbulent environments. Only chains with specialized structures, such as spaces between the cells, can overcome this disadvantage and even obtain a higher nutrient supply than do solitary cells. The model results are compared to laboratory measurements of nutrient uptake under turbulent conditions and to effects of sinking.

Diatoms have developed various cell shapes as well as chains of a variety of different structures and sizes. Of the many possible functions of chain formation, Fryxell and Miller (1978) summarized protection from grazing, increased concentrations of possible growth factors, improved fertilization possibilities, and changes in the sinking behavior. Here we consider impacts on potential diffusive and advective nutrient supply and uptake by differently shaped diatom cells and cell chains in a turbulent environment. Spherical and elongated solitary cells as well as cell chains are represented by prolate spheroids characterized by a small radius $c$ and an aspect ratio $r_a$ (Fig. 1). This restricts direct application of the results to solitary cells and compact, short cell chains of rather simple shape and approximately circular cross section. Expansion toward more complicated shapes and longer chains is possible only in a qualitative manner. All symbols are explained in Table 1.

At length scales larger than a few centimeters turbulent water motions produce a more or less homogeneous nutrient concentration distribution; however, at the much smaller scales of most phytoplankton, nutrient uptake can locally deplete the nutrients (Fig. 2) in the vicinity of the cells (Droop 1973). Nutrients are resupplied by diffusive and advective nutrient transport toward the cell surface (Fig. 2). Motions of phytoplankton cells or the water surrounding them can enhance the advective nutrient supply (Mann and Lazier 1991; Jumars et al. 1993; Kiørboe 1993; Karp-Boss et al. 1996). The relative contribution of advection to total transport is characterized by the nondimensional Péclet number *Pe*, defined as (Boucher and Alves 1959)

$$Pe = \frac{UL}{D},$$

where $U$ and $L$ are a characteristic velocity and length, respectively, and $D$ is the diffusivity. Both the diffusive and the advective nutrient transport are influenced by the shape of a phytoplankton organism (Crank 1975; Batchelor 1979; Karp-Boss et al. 1996). Owing to the dimensions of most phytoplankton cells, diffusion is much more effective than advection, and cell shape can influence nutrient uptake only by means of changing the nutrient concentration in the immediate vicinity of the cell surface (Berg and Purcell 1977). The total nutrient transport relative to purely diffusive transport is described by the nondimensional Sherwood number *Sh* (Boucher and Alves 1959). It is generally considered a function of *Pe* and is defined as unity in the absence of any water motions (e.g. Logan and Alldredge 1989; Karp-Boss et al. 1996). The relative increase in transport over pure diffusion due to advection is thus $Sh - 1$.

The smallest scale of turbulent motions is characterized by the Kolmogorov scale $L_v$:

$$L_v = \left(\frac{\nu^3}{\epsilon}\right)^{1/4}, \quad (1)$$

where $\nu$ and $\epsilon$ are the kinematic viscosity of seawater and the energy dissipation rate, respectively. The smallest turbulence scale is best described by $2\pi L_v$ (Lazier and Mann 1989), yielding, with $\nu = 10^{-6}$ m$^2$ s$^{-1}$ and $\epsilon$ ranging from $10^{-9}$ to $10^{-6}$ m$^2$ s$^{-3}$, a scale ranging from ~0.5 to 5 cm. At scales of less than $L_v$, characteristic of diatom cells, turbulence creates a linear shear (Lazier and Mann 1989), for which the characteristic velocity is $U = \dot{\gamma}L$, where $\dot{\gamma}$ is the shear rate. Therefore, a linear shear is assumed here to represent the immediate surrounding of diatoms in a turbulent environment. If the characteristic length $L$ for a prolate spheroid with small radius $c$ and aspect ratio $r_a$ is defined as the geometric mean radius, i.e. $L = c\sqrt{r_a}$, *Pe* can be defined as

$$Pe = \frac{\dot{\gamma} r_a c^2}{D}, \quad (2)$$

and $Pe/r_a$ is constant for chains with constant small radius.

*Acknowledgments*

We thank L. Karp-Boss and P. A. Jumars for very helpful ideas and comments and for pointing out an error in an earlier version of this manuscript. Our paper benefited from the comments of two anonymous reviewers. This is publication 1391 of the Alfred Wegener Institute for Polar and Marine Research.

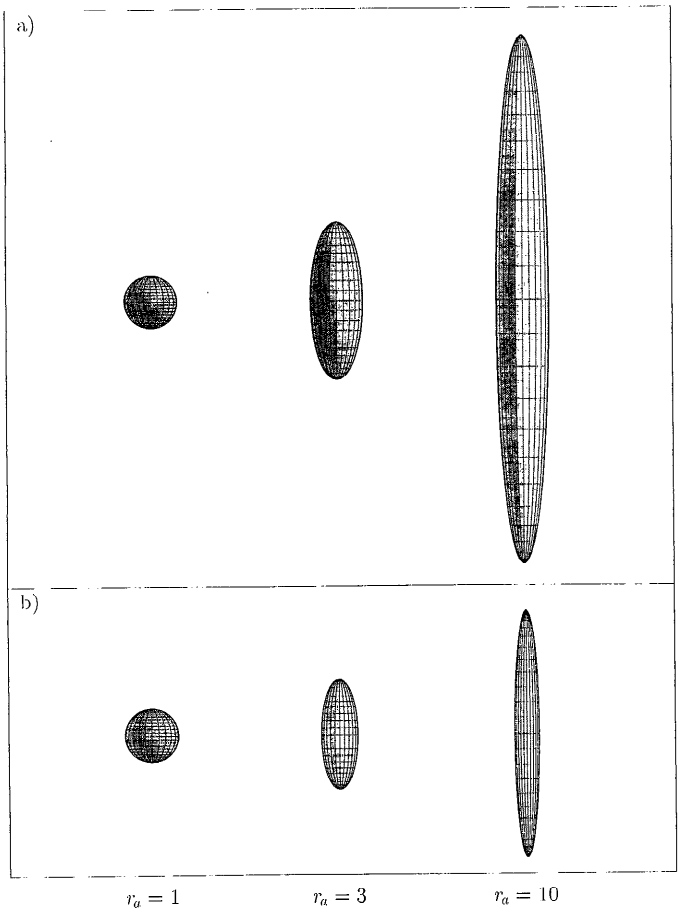


Fig. 1. Prolate spheroids of different aspect ratios $r_a$. Spheroids with constant small radius represent chains (a); their volume is proportional to $r_a$. Spheroids with constant volume simulate solitary elongated and spherical cells (b).

The relationship between cell shape, relative fluid motion, and nutrient supply was first examined theoretically by Munk and Riley (1952) who considered effects of turbulence negligible. For *Ditylum brightwellii,* Pasciak and Gavis (1975) directly observed an increased uptake rate at very high shear rates. Lazier and Mann (1989), using results from Purcell (1978), concluded that oceanic turbulence can significantly increase the nutrient supply of spherically shaped cells of at least 100-$\mu$m cell radius. Batchelor (1979) showed theoretically that the results of Purcell (1978) underestimated the advective transport for $Pe \ll 1$ and possibly also for larger $Pe$. Although chain formation also influences the sinking behavior of diatoms (Smayda 1970), effects of sinking are not examined herein. The influence of sinking (i.e. translational motion) on nutrient supply was examined by Berg and Purcell (1977).

Potential nutrient supply by means of diffusive and advective transport toward phytoplankton (i.e. the transport capacity $F_p$) sets an upper limit for the nutrient uptake. How much of this is actually used by a phytoplankton organism is then determined by its nutrient uptake kinetics (Fig. 2), as described by a Michaelis–Menten kinetics (Droop 1973):

Table 1. Symbols used in the text and their units.

| Symbol | Units | Meaning |
|---|---|---|
| $A$ | $m^2$ | Surface area |
| $c$ | m | Small radius of prolate spheroid |
| $C$ | mol $m^{-3}$ | Nutrient concentration |
| $C_0$ | mol $m^{-3}$ | $C$ at the cell surface |
| $C_0'$ | l | Relative $C_0$: $C_0' = C_0/C_1$ |
| $C_1$ | mol $m^{-3}$ | $C$ outside of the model region |
| $D$ | $m^2$ $s^{-1}$ | Diffusion coefficient |
| $D^*$ | $m^2$ $s^{-1}$ | Apparent diffusivity for spheroid with constant $C_0$, $C_1$ |
| $E_u$ | l | Relative utilization of increase in $F_p$ due to shear for actual uptake |
| $\epsilon$ | W $kg^{-1}$ | Turbulent energy dissipation rate |
| $\eta$, $\vartheta$, $\psi$ | l | Prolate spheroidal coordinates |
| $\eta_0$, $\eta_1$ | l | Innermost and outermost surfaces of model coordinate system |
| $f$ | m | Half the distance between the foci of a prolate spheroid |
| $F$ | mol $m^{-2}$ $s^{-1}$ | Total nutrient transport towards and through the cell surface |
| $F'$ | l | Nutrient flux to a chain relative to that of a solitary cell |
| $F_D$ | mol $m^{-2}$ $s^{-1}$ | Diffusive transport |
| $F_{D,C_0=0}$ | mol $m^{-2}$ $s^{-1}$ | Diffusion capacity, i.e. potential diffusive transport |
| $F_{D,r_a=1}$ | mol $m^{-2}$ $s^{-1}$ | $F_D$ for spheres |
| $F_{\max}$ | mol $m^{-2}$ $s^{-1}$ | Uptake capacity per unit of cell surface |
| $F'_{\max}$ | l | Relative $F_{\max}$: $F'_{\max} = F_{\max}/F_D$ |
| $F_p$ | mol $m^{-2}$ $s^{-1}$ | Transport capacity, i.e. potential diffusive and advective transport |
| $F_u$ | mol $m^{-2}$ $s^{-1}$ | Actual nutrient uptake per unit surface |
| $F'_u$ | l | Relative actual nutrient uptake |
| $F'_{u,D}$ | l | $F'_u$ for purely diffusive transport: $F'_{u,D} = F_u/F_D$ |
| $F'_{u,p}$ | l | $F'_u$ with respect to transport capacity: $F'_{u,p} = F_u/F_p$ |
| $\dot{\gamma}$ | $s^{-1}$ | Shear rate; velocity gradient |
| $K_M$ | mol $m^{-3}$ | Half-saturation constant; Michaelis constant; $F_{C_0=K_M} = F_{\max}/2$ |
| $K'_M$ | l | Relative $K_M$: $K'_M = K_M/C_1$ |
| $L$ | m | Characteristic length |
| $L_v$ | m | Kolmogorov length |
| $\nabla$ | $m^{-1}$ | Nabla vector; gradient |
| $\nabla_s$ | $m^{-1}$ | Gradient outward normal to the cell surface |
| $\nu$ | $m^2$ $s^{-1}$ | Kinematic viscosity |
| $Pe$ | l | Péclet number |
| $\phi$, $\theta$ | l | Space angles of orientation of spheroid in a shear field |
| $P_o$ | l | Orbital parameter (Kim and Karrila 1991) |
| $r_a$ | l | Aspect ratio of spheroid |
| $Sh$ | l | Sherwood number; $Sh = F/F_D$ |
| $Sh_{\text{eff}}$ | l | Ratio of actual uptake $F_u$ over uptake for purely diffusive transport |
| $t$ | s | Time |
| $T$ | s | Period of Jeffery orbit |
| $\boldsymbol{v}$ | m $s^{-1}$ | Velocity vector of relative flow field |
| $u$ | m $s^{-1}$ | Sinking rate |
| $U$ | m $s^{-1}$ | Characteristic velocity |
| $V$ | $m^3$ | Volume |
| $V_{\max}$ | mol $cell^{-1}$ $s^{-1}$ | Maximal uptake rate per cell |
| $\boldsymbol{x}$ | m | Vector of point in space |

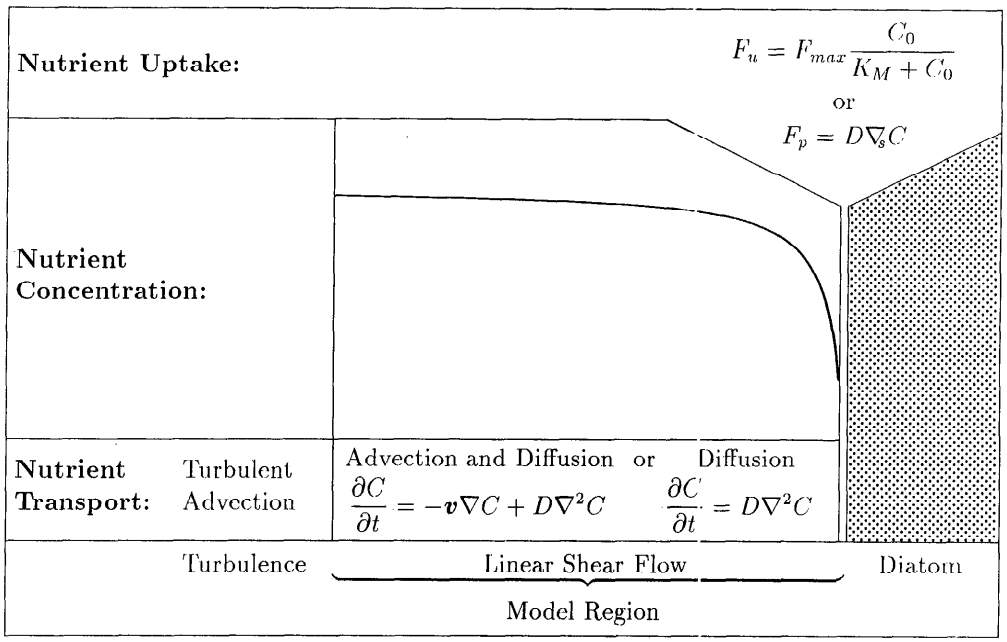


Fig. 2. Conceptual model diagram illustrating the processes involved in nutrient transport and uptake along with the governing equations. $C$ is the ambient, $C_0$ the cell surface nutrient concentration, $D$ the diffusivity, $F_p$ potential nutrient supply, $F_u$ actual nutrient uptake, $F_{max}$ maximum uptake capacity, $K_M$ half-saturation constant, and $\nabla_s$ the outward normal nutrient concentration gradient.

$$F_u = F_{max}\frac{C_0}{C_0 + K_M}, \tag{3}$$

where $F_u$ and $F_{max}$, $K_M$, and $C_0$ are the actual and maximal uptake rate (or uptake capacity) per unit of surface area, the half-saturation constant, and the nutrient concentration at the cell surface, respectively. Instead of the more commonly used maximal uptake rate per cell $V_{max}$, here we consider the uptake and transport rates per unit surface area in order to differentiate more clearly the various effects of cell shape on the surface : volume ratio, the diffusion capacity, and the transport capacity. The results can be easily related to cell volume by multiplying with the surface : volume ratio. However, biomass is not necessarily proportional to cell volume (Montagnes and Berges 1994), especially for diatom cells, which are to a large extent occupied by a vacuole, surrounded by a ~1-$\mu$m-thick cytoplasm layer (Strathmann 1967). The fact that phytoplankton cannot perfectly absorb all of the nutrients that diffusion and advection are able to supply to them also means that the cells can only partially utilize increases in the transport capacity (Pasciak and Gavis 1974, 1975). Obviously, if transport capacity is already much greater than uptake capacity, uptake cannot be improved by increasing transport capacity.

## The model

The following model describes nutrient uptake of diatom chains or elongated cells in a turbulent environment. At first the effect of the shape on purely diffusive nutrient transport is examined, then advection is included, and finally we consider the impact of uptake kinetics.

In this model, prolate spheroids serve as approximations to simulate shapes of chains or elongated cells (Fig. 1). Chains, on the one hand, are represented by spheroids of constant small radius $c$, whose volume is proportional to the aspect ratio $r_a$ (Fig. 1a), thus $r_a$ stands for the number of cells in a compact chain. Solitary cells, on the other hand, are modeled as spheroids of constant volume (Fig. 1b). Therefore, chains are compared with solitary cells of the same small radius but much smaller volume, whereas elongated solitary cells are compared with spherical cells of the same volume. The surface area $A$ and volume $V$ of a prolate spheroid are given by

$$A = 2\pi c^2\left(1 + \frac{r_a^2}{\sqrt{r_a^2 - 1}}\arcsin\sqrt{1 - \frac{1}{r_a^2}}\right),$$
$$V = \frac{4}{3}\pi r_a c^3. \tag{4}$$

The space around a prolate spheroid is represented by orthogonal prolate spheroidal coordinates (Moon and Spencer 1961):

$$\boldsymbol{x} = \begin{pmatrix} f\sinh\eta\sin\vartheta\cos\psi \\ f\sinh\eta\sin\vartheta\sin\psi \\ f\cosh\eta\cos\vartheta \end{pmatrix}, \tag{5}$$

where $f$ is half the distance between the two focal points of the spheroid and $\eta$, $\vartheta$, and $\psi$ are the prolate spheroidal coordinates. $\eta$ is in the outward direction and $\vartheta$ and $\psi$ are along the long and short axis of the spheroid, respectively. The innermost prolate spheroidal surface, i.e. the surface of

the organism, is then defined by $\eta_0 = \text{arcoth } r_a$, where $r_a$ is the aspect ratio of the organism. The outermost surface of the coordinate system is a spheroid with a small radius of $100c$. Because of the way the coordinates are defined in Eq. 5, the outermost surface, defined by $\eta_1$, is almost spherical ($r_a < 1.1$ for a grid radius of $100c$). For cell radii typical of diatom cells, although $100c$ is smaller than the smallest scale of turbulent water motions, at this distance advection usually is much more efficient than diffusion in terms of nutrient transport.

*Diffusion*—For purely diffusive nutrient transport the concentration distribution can be obtained as the analytical solution of the diffusive equation (Crank 1975):

$$\frac{\partial C}{\partial t} = D\nabla^2 C, \tag{6}$$

where $C$ and $D$ are the concentration and the diffusivity, respectively. In prolate spheroidal coordinates the nabla operator $\nabla$ takes the form (Moon and Spencer 1961):

$$\nabla = \frac{1}{f}\begin{pmatrix} \dfrac{1}{\sqrt{\sinh^2\eta + \sin^2\vartheta}}\dfrac{\partial}{\partial\eta} \\ \dfrac{1}{\sqrt{\sinh^2\eta + \sin^2\vartheta}}\dfrac{\partial}{\partial\vartheta} \\ \dfrac{1}{\sinh\eta\sin\vartheta}\dfrac{\partial}{\partial\psi} \end{pmatrix}. \tag{7}$$

In the case of a nutrient distribution independent of $\vartheta$ and $\psi$ (i.e. constant nutrient concentrations along surfaces defined by constant $\eta$ around the spheroid), the solution of Eq. 6 is (Moon and Spencer 1961):

$$C = \frac{C_0 \ln\tanh\left(\frac{\eta_1}{2}\right) - C_1 \ln\tanh\left(\frac{\eta_0}{2}\right) + (C_1 - C_0)\ln\tanh\left(\frac{\eta}{2}\right)}{\ln\left[\tanh\left(\frac{\eta_1}{2}\right)\coth\left(\frac{\eta_0}{2}\right)\right]}, \tag{8}$$

where $C_0$ and $C_1$ are the nutrient concentrations at the innermost and outermost surfaces of the coordinate system defined by $\eta_0$ and $\eta_1$, respectively. The diffusive nutrient transport $F_D$ toward the cell surface is given by the diffusion equation (Crank 1975):

$$F_D = -D\nabla_1 C. \tag{9}$$

From Eq. 5, 7–9, and with

$$D^* = \frac{4\pi c^2 D\sqrt{r_a^2 - 1}}{A \ln\left[\coth\left(\frac{\eta_0}{2}\right)\tanh\left(\frac{\eta_1}{2}\right)\right]}, \qquad \eta_0 = \text{arcoth } r_a, \quad \lim_{r_a\to 1} D^* = D, \tag{10}$$

we obtain (for constant $C_0$, $C_1$)

$$F_D = \frac{D^*}{c}(C_1 - C_0), \tag{11}$$

and the diffusion capacity (i.e. potential diffusive transport) is obtained as $F_{D,C_0=0}$.

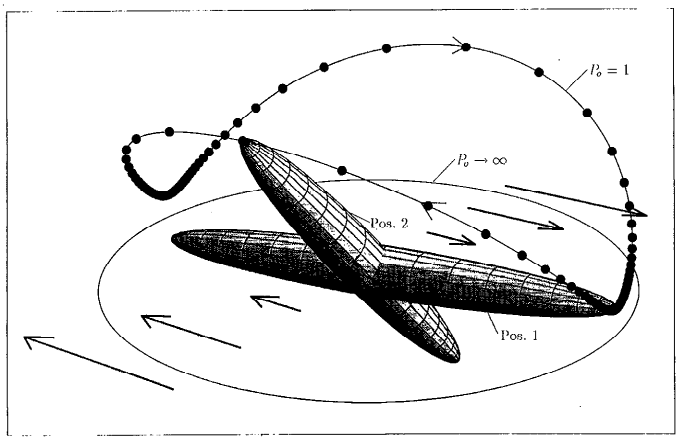


Fig. 3. Jeffery orbits. A spheroid is shown in two positions: Pos. 1 in relative quiescence; Pos. 2 at highest velocity while turning around. The intervals between the points on the upper Jeffery orbit are constant (~0.5 s for the spheroid shown and a shear rate of 1 $s^{-1}$). The bold arrows indicate the shear flow. The orbital parameter, $P_o$, determines the actual Jeffery orbit followed by the spheroid.

*Advection*—The total nutrient transport also involves advection and the relationship between total transport capacity $F_p$ and diffusion capacity $F_{D,C_0=0}$ is, using the above definition of *Sh*,

$$F_p = ShF_{D,C_0=0}. \tag{12}$$

The concentration distribution is governed by the diffusion advection equation

$$\frac{\partial C}{\partial t} + \boldsymbol{v}\nabla C = D\nabla^2 C, \tag{13}$$

where $\nabla$ is the same as above. The velocity field $\boldsymbol{v}$ in Eq. 13 is the relative flow of the water with respect to the spheroid, which itself also moves, as opposed to absolute flow, here denoting flow with respect to the shear direction. Hence the relative flow is obtained by subtracting the spheroid's motion from the absolute velocity field.

The motion of a spheroid in a shear field follows intermittent trajectories, so-called Jeffery orbits (Fig. 3). They are defined by (Kim and Karrila 1991, modified)

$$\tan\theta = \frac{P_o r_a}{\sqrt{r_a^2\sin^2\phi + \cos^2\phi}}$$

$$\cot\phi = -r_a\cot\left(\frac{\dot\gamma t}{r_a + r_a^{-1}}\right),$$

where $P_o$ is the orbital parameter (Fig. 3). The period $T$ of a Jeffery orbit depends on the aspect ratio and the shear rate

$$T = \frac{2\pi}{\dot\gamma}(r_a + r_a^{-1}). \tag{14}$$

The solution for the absolute flow past a torque-free prolate spheroid immersed in a linear shear flow (Fig. 4a, b, c, e) was given by Kim and Karrila (1991). Because of the intermittency of the Jeffery orbits, the relative flow (Fig. 4d,

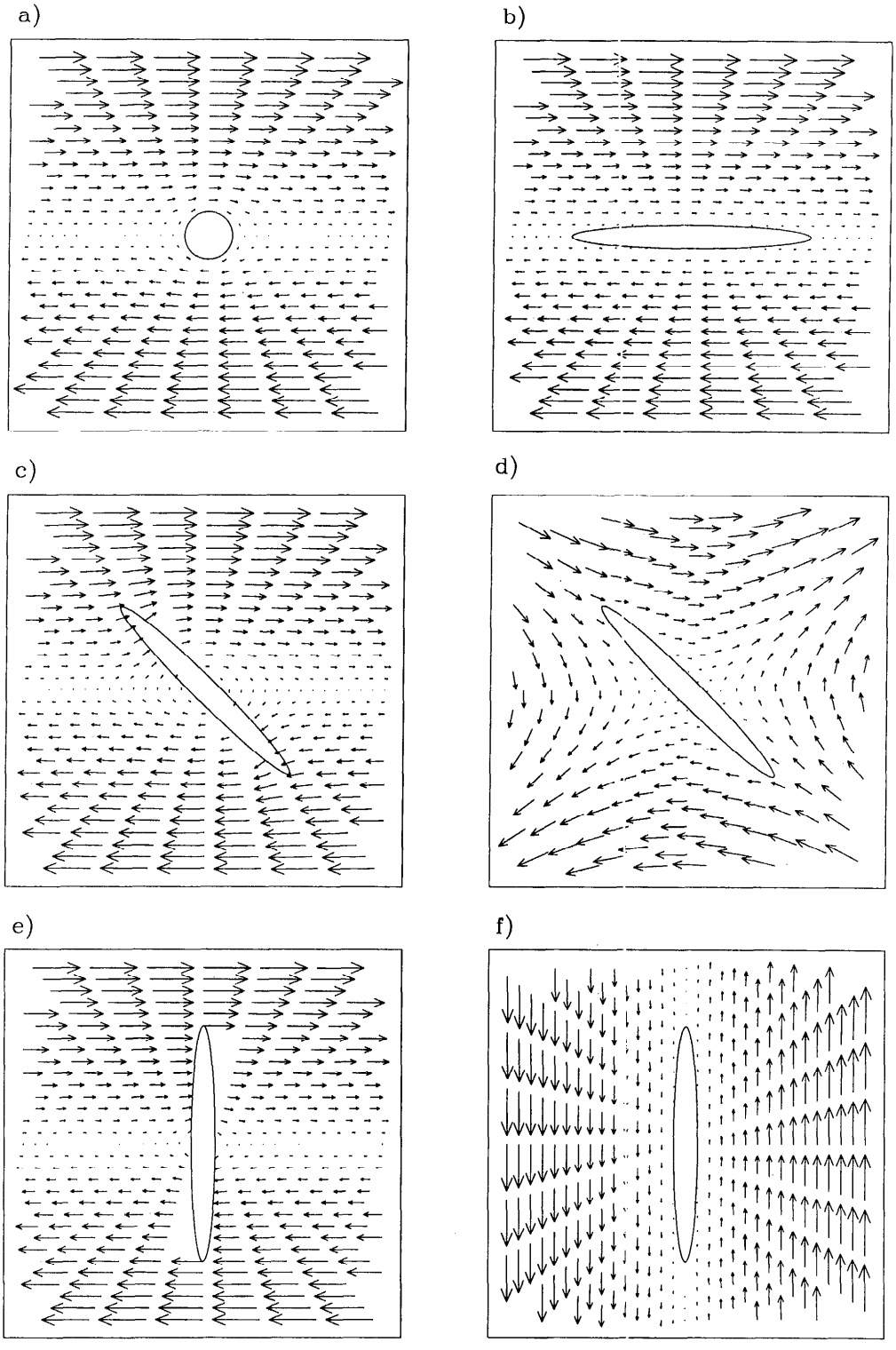


Fig. 4. Velocity field around a sphere (a) and a prolate spheroid in different orientations (b, c, e) in a linear shear. (d, f) Relative velocity field, i.e. with respect to a fixed spheroid, for the same conditions as in panels c and e. (d, f) Obtained by subtracting the motion of the spheroid from the fluid motion shown in panels c and e. Panel a is also the velocity field around a prolate spheroid oriented with its long axis perpendicular to the shear flow. Relative velocity for panel a looks similar to panel d. Relative and absolute velocities for panel b are almost the same, because in this orientation the spheroid moves very slowly. The orientation in panel b corresponds to Pos. 1 in Fig. 3; that in panels e and f to Pos. 2. The orientation in panels c and d is intermediate. Here, absolute flow is the flow with respect to the shear direction, and relative flow is with respect to the moving spheroid.

f) changes drastically as the spheroid turns around. For example, when its long axis is aligned to the shear (Fig. 3, pos. 1 and Fig. 4b), the spheroid moves very slowly and the relative and absolute flow fields are almost identical. The more the spheroid moves out of alignment with the shear, the more quickly it turns around (Fig. 3, pos. 2 and Fig. 4c–f).

Using the relative flow $\nu$, Eq. 13 was discretized using the implicit Crank–Nicolson finite difference scheme (Crank 1975) using 150, 62, and 62 grid points in the $\eta$, $\vartheta$, and $\psi$ direction, respectively. The small radius and aspect ratio of the outermost grid surface were $100c$ and $<1.1$, respectively. Due to the use of prolate spheroidal coordinates, grid resolution was finer at the tips of the spheroid than near the small equator and finer at the innermost grid surface than farther away from the spheroid. The following numbers are for the two innermost grid surfaces. In the $\eta$ direction, grid resolution ranged from $0.013c$ (independent of $r_a$) over the tip to $0.03c$ ($r_a = 1$) to $0.2c$ ($r_a = 10$) over the small equator. Grid resolution in $\vartheta$ and $\psi$ directions was $0.05c$ and $0.003c$ over the tip to $0.05r_ac$ and $0.1c$ over the small equator, respectively. The resulting system of equations was solved with the SOR method (Press et al. 1992). Initially, for each run the spheroid was fixed to the position aligned to the shear (Fig. 3, pos. 1). Convergence of the solution for this position was assumed if $F_p$ differed less than $0.0005F_p$ over a timespan of $3T$, because longer calculations did not reduce variations in $F_p$ further. Thereafter, one-half rotation (lasting $T/2$) of the spheroid following a Jeffery orbit was simulated. Averages were computed by dividing the total transport over one-half rotation by $T/2$.

*Uptake kinetics*—Until now, nutrient concentrations at the outer ($\eta = \eta_1$) and inner ($\eta = \eta_0$) surfaces of the coordinate system have been assumed constant. As mentioned above, however, for real phytoplankton the cell surface nutrient concentration $C_0$ is determined by both potential nutrient supply as well as the organism's uptake kinetics. In order to estimate how far uptake kinetics affect utilization of increased nutrient transport capacity, we first need to derive expressions for uptake kinetics normalized to potential ambient nutrient supply. Looking at diffusion alone, nutrient uptake at the cell surface, Eq. 3, must equal the diffusive transport, Eq. 9 and 11:

$$\frac{D^*}{c}(C_1 - C_0) = F_{\max}\frac{C_0}{K_M + C_0}. \tag{15}$$

If we define as dimensionless quantities a relative cell surface nutrient concentration $C'_0$, a relative maximal uptake capacity $F'_{\max}$, and a relative half saturation constant $K'_M$ as

$$C'_0 = \frac{C_0}{C_1}, \quad F'_{\max} = \frac{F_{\max}}{F_{D,C_0=0}} = \frac{cF_{\max}}{D^*C_1}, \quad \text{and} \quad K'_M = \frac{K_M}{C_1}, \tag{16}$$

Eq. 15 can be transformed into

$$1 - C'_0 = F'_{\max}\frac{C'_0}{K'_M + C'_0}, \tag{17}$$

which describes a relative nutrient uptake kinetics with respect to ambient diffusion capacity and nutrient concentration. The actual nutrient uptake relative to the diffusion capacity is defined as

$$F'_{u,D} = \frac{F_u}{F_{D,C_0=0}} = \frac{cF_u}{D^*C_1}. \tag{18}$$

Solving Eq. 17 for $C'_0$ and substituting into Eq. 3 yields

$$F'_{u,D} = F'_u(F'_{\max}, K'_M) = \frac{1 + K'_M + F'_{\max}}{2} - \sqrt{\left(\frac{1 - K'_M - F'_{\max}}{2}\right)^2 + K'_M} \tag{19}$$

(obviously, $C'_0$ is not a constant, here, but the error in $F'$ because of this simplification is $\ll 1\%$ for the range of values used in this paper, so Eq. 19 can be considered accurate). With respect to these equations, describing uptake at the cell surface, the means of nutrient transport (i.e. diffusion or advection) should not matter. Reformulating the expression for $F'_{\max}$ in Eq. 16 with the help of Eq. 12 shows that larger Sherwood numbers correspond to lower relative maximal uptake capacities:

$$\frac{F_{\max}}{F_p} = \frac{F_{\max}}{ShF_{D,C_0=0}} = \frac{F'_{\max}}{Sh}. \tag{20}$$

Thus, relative actual nutrient uptake with respect to the total potential transport capacity $F'_{u,p}$ is obtained by replacing $F'_{\max}$ with $F'_{\max}/Sh$, in Eq. 19, which is described by

$$F'_{u,p} = \frac{F_u}{F_p} = \frac{F_u}{ShF_{D,C_0=0}} = F'_u\left(\frac{F'_{\max}}{Sh}, K'_M\right). \tag{21}$$

If we denote as the effective Sherwood number $Sh_{\text{eff}}$ the ratio of actual uptake over uptake in the absence of advection, it follows from Eq. 18 and 21 that

$$Sh_{\text{eff}} = \frac{ShF'_{u,p}}{F'_{u,D}} = Sh\frac{F'_u\left(\frac{F'_{\max}}{Sh}, K'_M\right)}{F'_u(F'_{\max}, K'_M)}. \tag{22}$$

The utilization efficiency $E_u$ of a given Sherwood number (i.e. how much of the relative increase in transport capacity shows up as a relative increase in actual uptake) can then be defined by the ratio

$$E_u = \frac{Sh_{\text{eff}} - 1}{Sh - 1}. \tag{23}$$

Because relative maximal uptake capacities with respect to total transport capacity will always be lower for greater Sherwood numbers, $E_u$ will as well be decreased by advection.

## Results

*Influence of shape on diffusion*—The shape of a phytoplankton organism can influence diffusive transport in two ways, first by changing the surface area : volume ratio and second by affecting the diffusive nutrient transport per unit of surface area. An elongated, solitary cell has a much great-

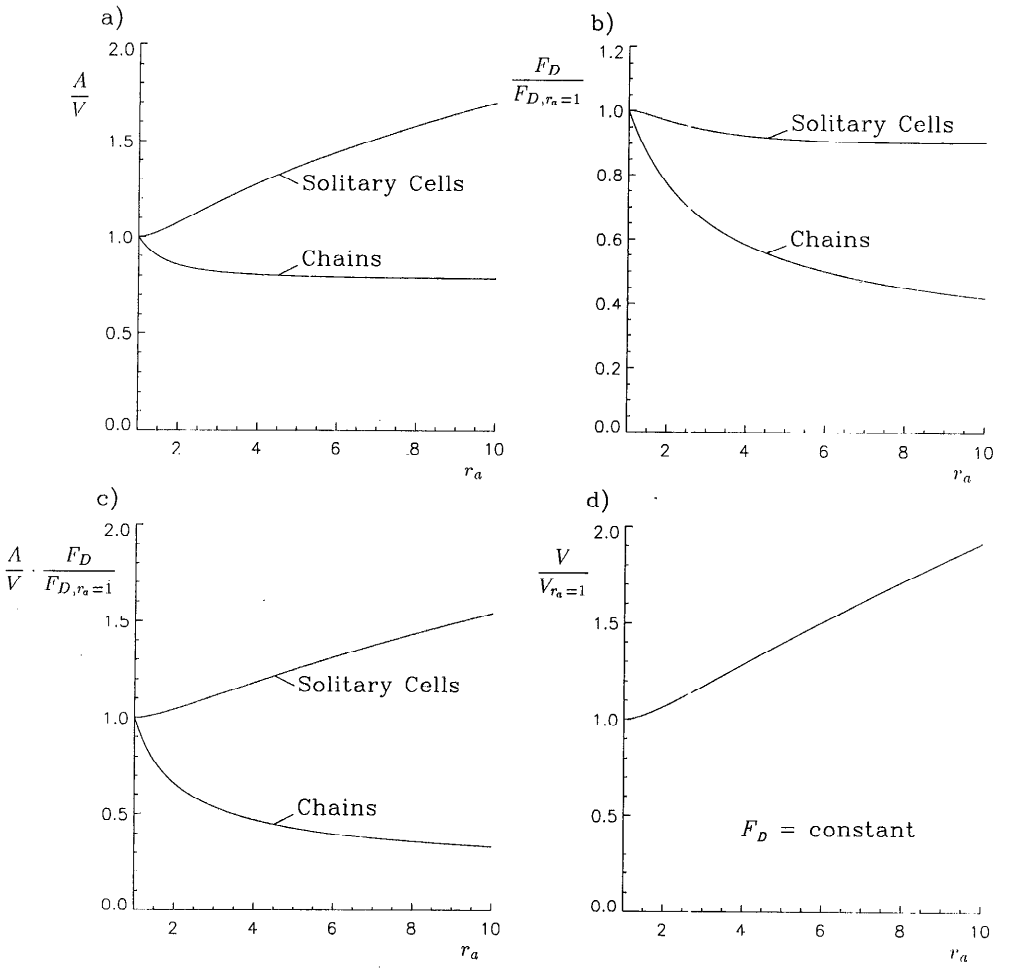


Fig. 5. Effects of aspect ratio $r_a$ on diffusive transport and surface area : volume ratio. (a) Surface area : volume ratio $A/V$. (b) Relative diffusive transport per unit of surface area $F_D/F_{D,r_a=1}$ as a function of the aspect ratio $r_a$ for spherical and elongated solitary cells of constant cell volume as well as cell chains with constant cell radius. (c) Relative diffusive transport per unit volume, expressed as the product of panels a and b, $A/V \times F_D/F_{D,r_a=1}$; panel b was obtained from Eq. 11. (d) Volume of elongated cells $V$ relative to volume of a spherical cell $V_{r_a=1}$ achieving the same diffusive nutrient supply per unit volume.

er surface area than a spherical cell of the same volume (Fig. 5a), resulting in improved diffusive nutrient transport per cell, although the diffusive nutrient supply per unit of surface area is reduced (Fig. 5b, upper curve). Conversely, cells in a chain, the volume of which is proportional to its aspect ratio $r_a$, suffer a decrease both in surface area (Fig. 5a) and diffusive transport per unit of surface area (Fig. 5b, lower curve). In combination, both effects lead to a strong difference between elongated solitary cells and cell chains in diffusive supply per unit volume, i.e. per cell (Fig. 5c). For example, whereas a solitary cell with an $r_a$ of 10 enjoys a 54% higher diffusive nutrient supply per cell than does a spherical cell of the same volume, the cells of a chain of the same aspect ratio reach only one-third of the diffusive transport that they would get as solitary cells (Fig. 5c). For solitary cells, this also means that an elongated cell can have a greater volume than a spherical cell for the same diffusive transport (Fig. 5d). It can also be derived from Fig. 5 that the reduction in diffusion due to chain formation is less pronounced if the chain consists of elongated cells. In summary, for solitary cells of a given volume an elongated shape offers great advantage, whereas chain formation is disadvantageous with respect to diffusive nutrient supply.

*Shape effects on advection*—As mentioned above, a spheroid in a linear shear field rotates intermittently. Consequently, there is a corresponding intermittency in potential nutrient supply $F_p$ (Fig. 6). All results concerning the relationships among advection, cell shape, and nutrient supply are obtained from the numerical simulations and are averages over one-half rotation along a Jeffery orbit with $P_o = 1$.

The advective contribution to nutrient transport can be represented by the relative increase in the transport capacity over pure diffusion due to advection, as given by $Sh - 1$. For chains, represented by spheroids of constant small radius

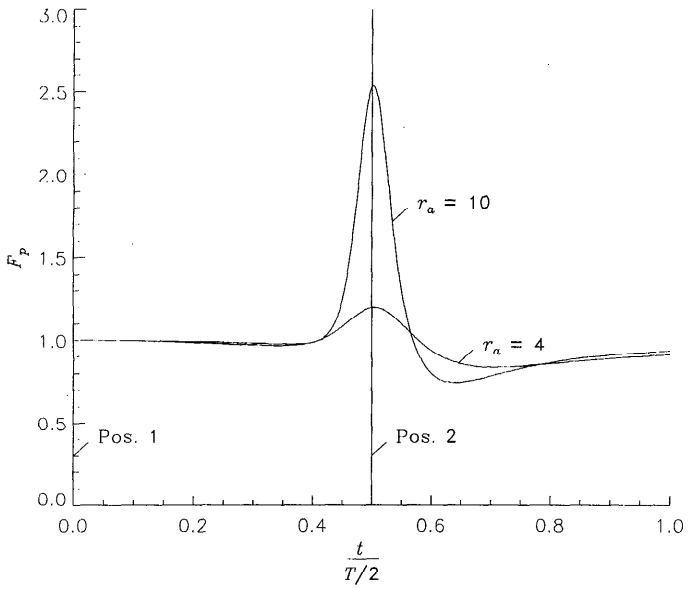


Fig. 6. Time course of the transport capacity $F_p$ in arbitrary units over one-half rotation along a Jeffery orbit for two different aspect ratios $r_a$, with $P_o = 1$ and $Pe/r_a = 1$. Pos. 1 and 2 correspond to the two positions of the spheroid in Fig. 3. The conspicuous spike in $F_p$ exists only for Jeffery orbits with $P_o$ significantly different from 0.

$c$, the relative increase in transport capacity $Sh - 1$ is much stronger for longer as well as (because larger $c$ leads, via Eq. 2, to larger $Pe$) for thicker chains (Fig. 7). For solitary cells of constant volume, on the other hand, the impact of advection is only very weakly (on the order of 20% in $Sh - 1$ or 2% in $Sh$) affected by cell shape for $r_a = 1 \ldots 10$ (not shown). Thus, at least for large cells or strong turbulence, the small-scale linear shear has a much greater effect on the nutrient supply of chains than of solitary cells (Fig. 7).

The important question, however, is whether the greater advective supply to chains can compensate the reduced diffusive transport. The answer is obtained by combining the effects of chain formation on diffusion (Fig. 5b) and advection (Fig. 7), yielding a direct comparison of the nutrient supply for solitary cells and compact cell chains in a turbulent environment (Fig. 8). Clearly, the larger increase in total nutrient supply due to turbulence for chains cannot compensate the loss in diffusive transport. This means that a solitary cell will always enjoy a greater nutrient supply than will a cell in a compact chain, as long as the (not necessarily spherical) shape of the individual cells of the chain is the same as that of the solitary cell. The reduction in nutrient supply per unit volume (i.e. per cell) due to chain formation (Fig. 5b, c) is even stronger than per unit of surface area (Fig. 8). Note that this conclusion would not be valid the other way around, i.e. a decreased supply per unit volume does not necessarily mean a decrease per unit surface. Therefore, the comparison was done per unit of surface

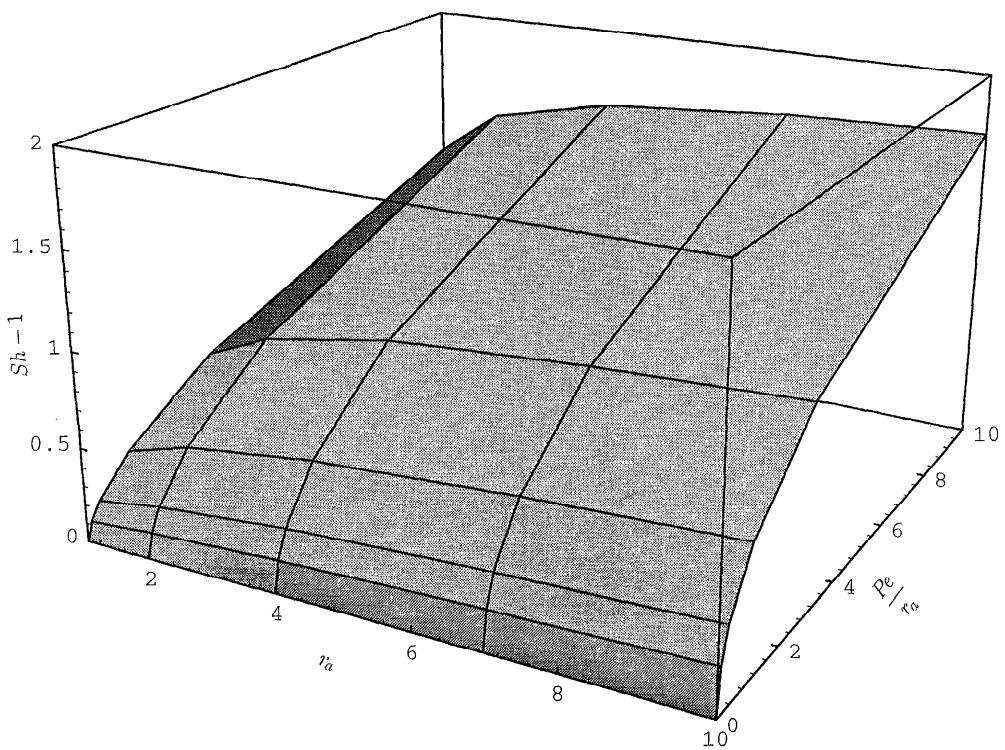


Fig. 7. Relative increase in transport capacity $Sh - 1$ due to shear flow for cells in a chain as a function of aspect ratio $r_a$ and Péclet number $Pe$. $Pe$ can be converted to actual cell sizes $c$ and shear rates $\dot{\gamma}$ via Eq. 2; $r_a$ represents the number of cells in a chain.

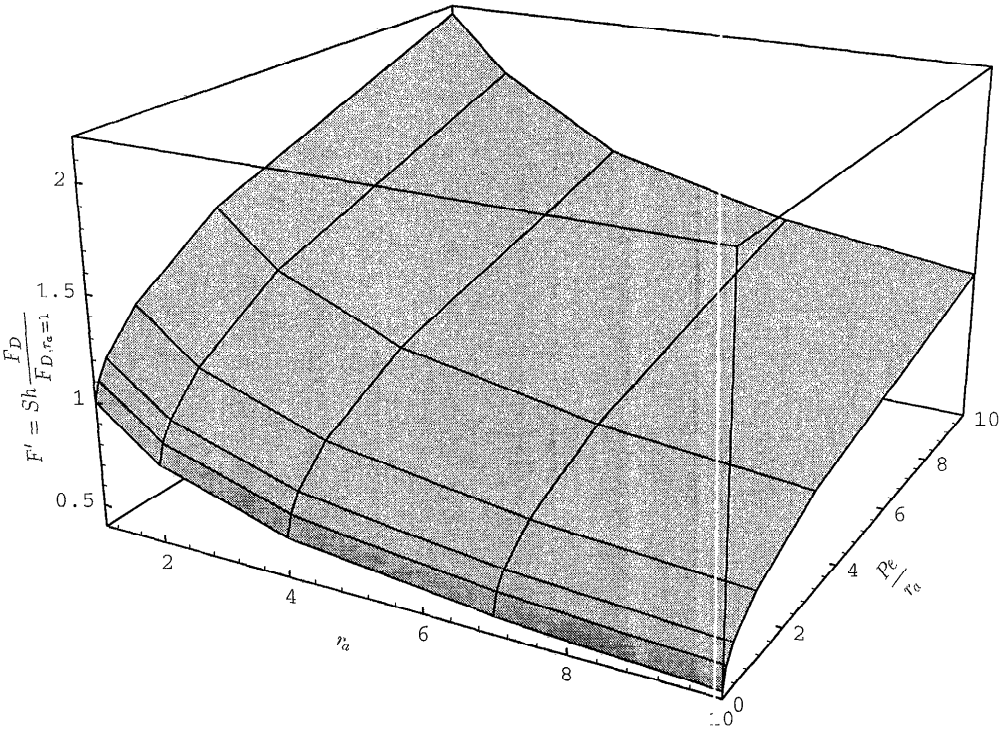


Fig. 8. Relative total nutrient transport $F'$, expressed as the product of Sherwood number and relative diffusive transport $Sh$ ($F_D/F_{D,r_a=1}$), for chains and single spherical cells as a function of aspect ratio $r_a$ and Péclet number $Pe$ for the same conditions as in Fig. 7. This graph is a combination of Fig. 7 and the lower curve in Fig. 5b.

area. On the other hand, even if volume is to represent biomass, the conclusion of reduced potential total transport depends on chain morphology (*see discussion*).

*Impact of uptake kinetics*—Relative utilization efficiency $E_u$ of a relative increase in potential nutrient supply $Sh - 1$ is a function of three factors: relative half-saturation constant $K'_M$, relative uptake capacity $F'_{max}$, and the Sherwood number $Sh$ (Fig. 9). Measured values reported by Pasciak and Gavis (1974, 1975) for $K_M$ and $F_{max}$ for nitrate show that uptake capacities are usually below the diffusion capacities (solid dots in Fig. 9).

The dependence of the relationship between $E_u$ and $F'_{max}$ is indicated by the point marked $Sh$ on the $F'_{max}$ axis in Fig. 9. It shows that it is easier (requires a lower relative uptake capacity) to utilize a small increase in potential nutrient supply than a large increase.

As one would expect, a higher relative uptake capacity $F'_{max}$ corresponds to a more efficient utilization of advective transport (rear part of Fig. 9). Interestingly, at least for uptake capacities in the range indicated by the dots, a higher relative half-saturation constant $K'_M$ can generally also weakly improve the utilization of a given Sherwood number (front part of Fig. 9). The influence of the ambient nutrient concentration is indicated by different sizes of the dots. For example, nitrate uptake of *D. brightwellii* (three dots marked D in the figure) shows that a significant utilization of an increase in potential nutrient supply due to advection can only occur at rather low nutrient concentrations.

*Sensitivity analysis*—Apart from the Péclet number and the uptake kinetics, two parameters can affect the model results. One is the size (diameter) of the model grid, and the other is the orientation of the spheroid relative to the shear field.

Because of Eq. 5, application of the model results to smaller cell sizes reduces the actual size of the model area in Fig. 2; i.e. the actual grid radius can become much smaller than the smallest turbulent length scale. A smaller domain leads to increased diffusion and decreased advection. The differences between chains and solitary cells are thereby reduced for small $Pe$ and enhanced for large $Pe$. Reduction of the domain radius from $100c$ to $10c$ can raise the total nutrient supply by almost 10%, the effect being most pronounced at low $Pe$. Increasing the grid radius to $1{,}000c$ affected nutrient supply and $Sh - 1$ by <1%. The longest period $T$, Eq. 14, was ~10 min ($\dot{\gamma} = 0.1$ and $r_a = 10$). When the change in $F_D$ over 30 min was $<0.0005F_D$ in the case of pure diffusion, which is analogous to the convergence criterion used for numerical calculations with the longest period, the deviation of the numerical procedure from the analytical solution, Eq. 11, was $\sim 0.001F_D$.

As the shear causing the intermittent motions along the Jeffery orbits is caused by turbulence, its direction is not constant but varies over time. An estimate of the time scale of these variations can be obtained from the lifetime of the smallest turbulent eddies, which was given by Mitchell et al. (1985) as $<0.5T$ (and even less for chains or elongated cells). Lazier and Mann (1989) argued that these lifetime

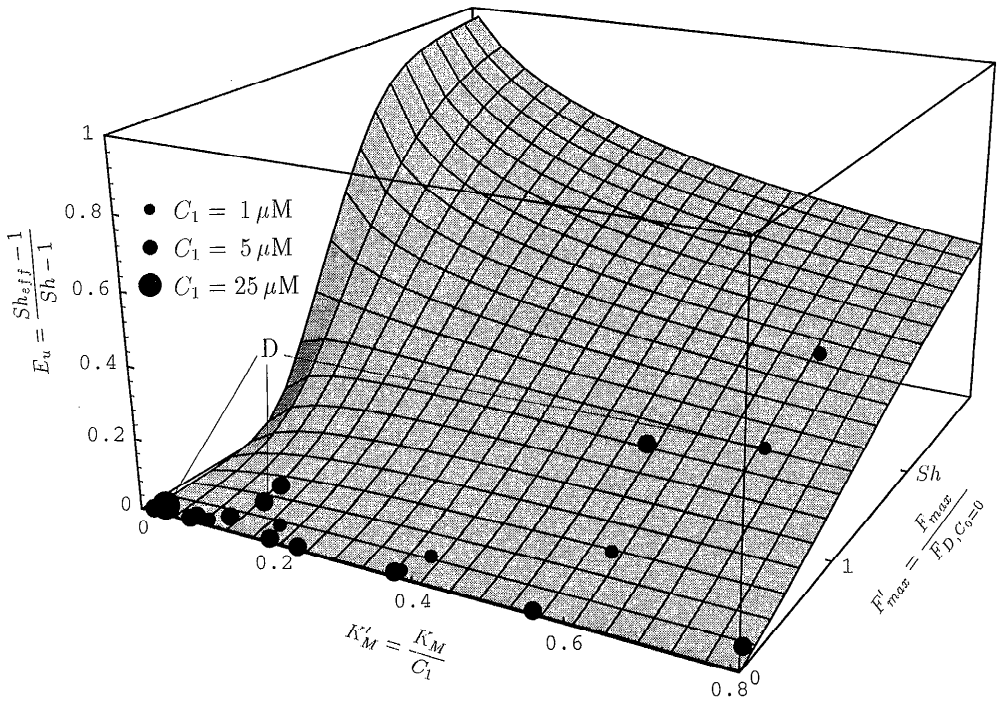


Fig. 9. Influence of nutrient uptake kinetics on the utilization efficiency $E_u$ of an increased transport capacity. $Sh - 1$ is the relative increase in transport capacity due to advection and $Sh_{eff} - 1$ is the relative increase in actual uptake. $E_u$ is plotted as a function of dimensionless relative half-saturation constant $K'_M$ and dimensionless relative uptake capacity $F'_{max}$. The points attached to the plotted surface are measured values of $K_M$ and $F_{max}$ from Pasciak and Gavis (1974, 1975) for nitrate uptake of different diatom species. The three points marked with D represent the same pair of $K_M$ and $F_{max}$ (of *Ditylum brightwellii*) for different nutrient concentrations. The point marked *Sh* on the $F'_{max}$ axis indicates the position on this axis where the relative uptake capacity $F'_{max}$ of the organism equals the Sherwood number. It shows the dependence of the relationship between $E_u$ and $F'_{max}$ on *Sh*.

estimates were too low by a factor of 10, i.e. a more realistic value should lie anywhere in between $0.5T$ and $5T$. In other words, the fluctuations in the shear direction would allow a spheroid to follow from one-half to several complete rotations along a certain Jeffery orbit before being switched to another by the changing shear field.

Although the intermittency of the Jeffery orbits and nutrient supply depend on $P_o$, the influence of $P_o$ on average $F_p$ is rather small (the greatest difference found was 3% in $Sh - 1$ for $r_a = 10$ and $Pe = 10$).

## Discussion

It is already known from previous research that the effect of advection on uptake is strongly size dependent (Munk and Riley 1952; Lazier and Mann 1989). Batchelor (1979) proved that the fractional increase in transport due to advection $Sh - 1$ is independent of the shape if the Péclet number $Pe$ is very small. From the present model we can conclude that the effect of a prolate shape on $Sh - 1$ remains small for $Pe$ up to 10.

For a stationary sphere in a steady simple shear flow, Batchelor (1979) reported that for $Pe \ll 1$ (in our notation)

$$Sh - 1 = 0.257\sqrt{Pe},$$

which, at least for the range of $Pe$ from 0.1 to 10 (Figs. 7, 8), yields $Sh$ differing by <2% (or $Sh - 1$ differing by <10%) from those calculated with the present model for spheres. An expansion of this formula toward elongated shapes was obtained empirically from the model results as

$$Sh - 1 = 0.363\sqrt{\frac{Pe}{r_a + 1}} + 0.115\frac{r_a - 1}{r_a + 1}Pe^{1/3}. \quad (24)$$

This formula reproduces the numerical results with a deviation of <10% from any result for $Sh - 1$ (Fig. 7) but should not be used to extrapolate the model results to larger (or smaller) values of $Pe$ or $r_a$.

*Application of the results to solitary cells and chains*—Basically, the present model can be applied both to pennate and centric diatoms. It is restricted, however, to free-living, pelagic cells. Thus, it cannot predict effects of elongated shapes on nutrient supply of benthic and attached cells, which live in the viscous sublayer adjacent to surfaces, with the flow around them being completely different from the one used here.

Application to chains is more complicated for two reasons. First, most diatom chains are much longer than 10 cell diameters, and second, most chains have structures very dif-

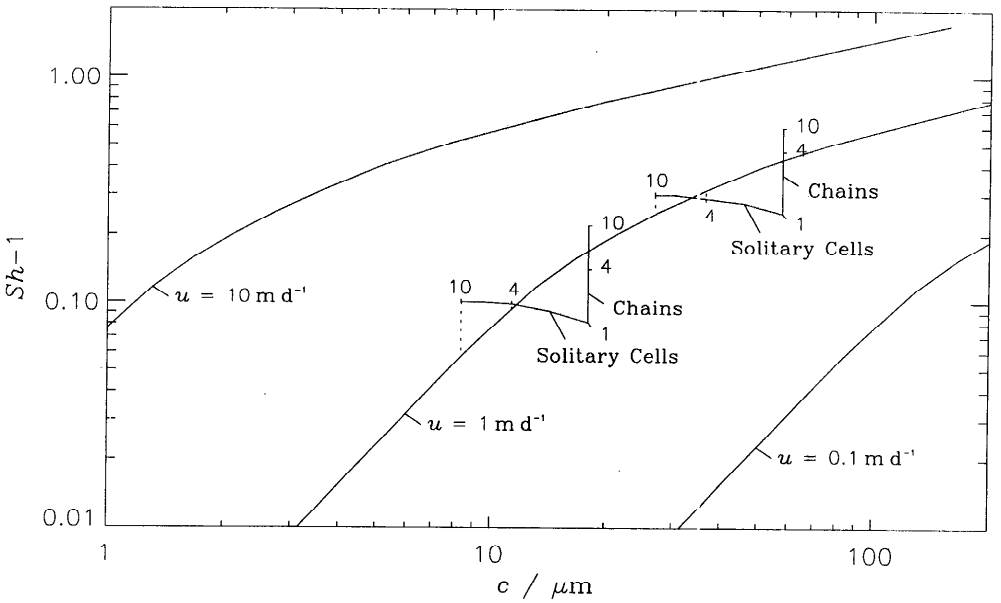


Fig. 10. Comparison of the influence of sinking with that of turbulence on potential nutrient supply of diatom cells and cell chains for a diffusion coefficient of $D = 2 \times 10^{-9}$ m$^2$ s$^{-1}$ (adapted from Lazier and Mann [1989] modified). The three long curves show the relative increase in nutrient supply $Sh - 1$ of solitary spherical cells due to low, intermediate, and high sinking velocities $u$ as a function of cell radius $c$, as given by Berg and Purcell (1977). The solid vertical lines show the relationship between relatively strong turbulence (with an energy dissipation rate of $\epsilon = 10^{-6}$ m$^2$ s$^{-3}$) and $Sh - 1$ for chains of constant cell radius. The curves extending to the left of the vertical lines give the same relationship for solitary cells of constant volume. The numbers on these lines indicate the aspect ratios. The dashed vertical lines indicate the difference between the effects of turbulence and moderate sinking rates.

ferent from compact, rigid, straight spheroids. Many chains (e.g. of *Skeletonema* sp. or *Thalassiosira* sp.) have large gaps between the cells. This could lead to the assumption that water can flow through these gaps (Karp-Boss et al. 1996). Because the spaces between the cells of diatom chains are not empty but contain the linking spines or threads, viscosity will to a large extent suppress such flows at these small dimensions, even if the cells sink rapidly (Koehl and Strickler 1981), similar to suppressing turbulence at scales of and below the Kolmogorov length $L_\nu$. Thus, we cannot expect the motional behavior of a chain with spaces between the cells to differ significantly from that of a solid chain. The gaps will merely act as to reduce the biomass per unit of chain length, which in turn will increase the nutrient supply for each cell. For example, if the spaces are about as long as the cells, the diffusive supply of a chain of five cells ($r_a$ = 9) will be much less reduced than without the gaps, i.e. to ~60% instead of 35% of the diffusive supply of a spherical solitary cell (Fig. 5c). Because of the impact of chain length on advection (Fig. 7), in a turbulent environment the total nutrient supply per cell can become much greater for cells in a chain with gaps than for solitary cells.

Similarly, again because of viscosity, long spines extending from the cell or chain surface will merely enlarge the size relevant for the flow, thereby reducing flow close to the cell surface. Because advection is much less efficient than diffusion close to the cell surface in any case, this reduction should not significantly affect the overall influence of advection on potential nutrient supply. Only if the cells have a large number of spines, distributed over the cell surface, could this strongly affect the Sherwood number.

The situation is different, however, if the chains are curved and flexible, not circular in cross section (as many ribbonlike chains of pennate diatoms), or extend almost as long or longer than the Kolmogorov length, in which cases the flow field will be completely different from that used in the present model. As relative velocities generally increase with increasing dimensions, one can only guess that very long chains may experience a significantly greater impact of advection than suggested by Fig. 7 (also see Karp-Boss et al. 1996).

In order to estimate the significance of shape effects on advective nutrient supply, the results of the present model can be compared with the effect of sinking (Fig. 10). As chain formation can increase as well as decrease sinking rates, depending on the species (Smayda 1970), a range of low to high sinking rates $u$ is used. Because sinking is a translational motion, results from Berg and Purcell (1977) for translating spheres (Fig. 10, three long curves) are compared to the effect of turbulence on nutrient supply (Fig. 10, short vertical and horizontal lines). The effect of turbulence is similar to that of moderate sinking rates. Both chain formation as well as cell elongation can strongly enhance the impact of turbulence relative to that of sinking on nutrient supply (vertical distance, as indicated by the dashed lines, in Fig. 10).

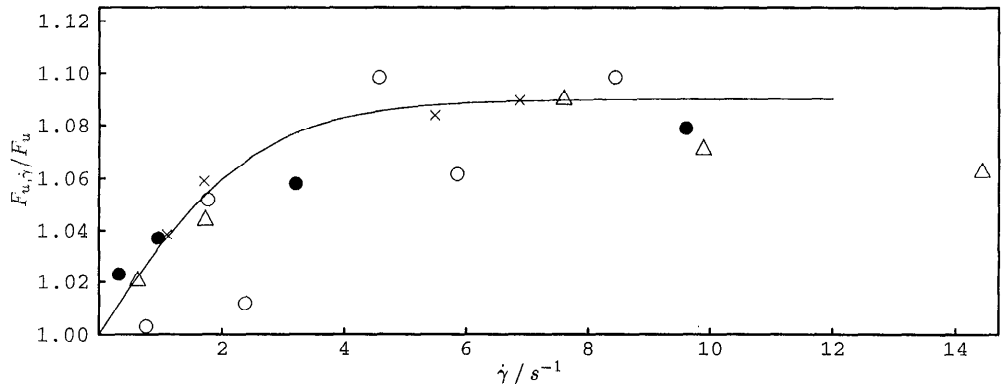


Fig. 11. Relative uptake of nitrate by *Ditylum brightwellii* as compared to uptake under purely diffusive nutrient supply as a function of shear (from Pasciak and Gavis [1975], fig. 5). Crosses and open symbols are measurements from Pasciak and Gavis; bold dots are results of the present model. The comparison of the model results (Fig. 7) with those of Pasciak and Gavis was done by converting Péclet numbers to shear rates via Eq. 2, using a small cell radius $c$ of 25 $\mu$m.

Several complications arise if one tries to implement uptake kinetics, e.g. in the current model. First, $F_{max}$ should not be considered constant (McCarthy 1981) but can vary even in less than a minute (Wheeler et al. 1982). Such short-term variations in uptake capacity could, in connection with intermittency of advective supply (Fig. 6), imply improved utilization of high *Sh*; i.e. Fig. 9 would underestimate the impact of turbulence on nutrient uptake. Second, because of the nutrient uptake, small nutrient-depleted zones form around each organism (Droop 1973; Pasciak and Gavis 1975). As $K_M$ cannot be measured directly at the cell surface, it is usually taken as the concentration in the surrounding medium, which leads to overestimates of unknown extent in this parameter (Harrison et al. 1989). Third, the uptake capacity seems to depend on the culture conditions of the algae. So Pasciak and Gavis (1974, 1975) published values from two separate sources for the uptake capacity of *D. brightwellii* differing by a factor of three.

There have been no experiments as yet on the differential nutrient uptake of chains vs. solitary cells in a turbulent environment. By use of a controlled shear apparatus, Pasciak and Gavis (1975) were able to measure nitrate uptake of *D. brightwellii,* which has an aspect ratio of 3, when exposed to a linear shear flow. A comparison of those measurements with the present model results, combining Figs. 7 and 9, is shown in Fig. 11. The model results appear to agree well with the measured values.

As the model results are a function of organism size and ambient shear rate, the significance of the predictions for a real bloom situation strongly depends not only on the uptake kinetics of the organisms but as well on observed size and kinetic energy spectra. Although several diatoms can become quite large, most species fall in the range below 25-$\mu$m cell radius. Small-scale shear from turbulence is a function of the turbulent energy dissipation rate $\epsilon$ as $\dot{\gamma} = \sqrt{\pi\epsilon/10\nu}$ (Lazier and Mann 1989). While shear rates as high as 10 $s^{-1}$ are sometimes taken as the upper limit found in marine environments (Pasciak and Gavis 1974; Shimeta et al. 1995), values between 0.01 and 1 $s^{-1}$ seem more common (Mitchell et al. 1985; Lazier and Mann 1989).

Uptake kinetic parameters of most phytoplankton, such as those shown in Fig. 9 for nitrate, would allow significant effects of shape on nutrient uptake to occur only for rather low nutrient concentrations (on the order of 1 $\mu$M in this case). Because chain formation decreases diffusive nutrient supply (Fig. 8), both high nutrient concentrations and strong turbulence are more favorable for chain formation. Because nutrient concentrations as well as turbulence are usually elevated at the beginning of a bloom (e.g. Valiela 1984; Gillbricht 1988; Kiørboe 1993), this means that at that time any possible advantages of chain formation (e.g. due to increased advective transport toward chains with gaps) would be most significant. Chain formation would be most disadvantageous, however, for the nutrient supply of larger phytoplankton toward the end of a bloom, when turbulence is weaker and nutrients are exhausted. This notion is supported by the finding of Smayda (1970) that chain length generally decreases under nutrient limitation, such as in aging batch cultures (Smayda 1966).

Smayda (1970) suggested that the curved shape and long spines of many diatom chains might infer rotation of the chains as they sink. Rotation of a chain along Jeffery orbits implies that chains rotate even if they are straight and if they do not sink. The strong intermittency of nutrient supply to longer chains or elongated cells (Fig. 6) could ease uptake for species adapted to higher concentrations during pulses of improved nutrient supply, thereby extending the possibility of efficient growth toward lower nutrient concentrations.

*Implications for shape evolution*—Because for solitary cells a prolate shape is always advantageous in terms of nutrient uptake, the question arises why so many phytoplankton, such as most small flagellates, are in fact of (almost) spherical shape. It could mean that such organisms are hardly ever diffusion limited in their environment; that is, diffusion limitation would not appear to be the primary evolutionary factor shaping phytoplankton cells. Because the impact of advection, caused by ambient turbulence, strongly depends on size (Fig. 7), it can be important only for the very largest phytoplankton species. Indeed, many of the larg-

er diatom species are strongly elongated. Taking again *D. brightwellii* as an example, we see from Fig. 7 that the transport capacity is increased in moderate turbulence ($\dot{\gamma} = 0.2$ $s^{-1}$) by ~20%, resulting in an improvement for actual nutrient uptake of <5% (Fig. 11).

In terms of chain evolution, the reduction in nutrient supply caused by chain formation has several implications. First, evolution of diatom chains seems to have started with compact, fused chains as in *Melosira* sp. (Beklemishev 1961). Support for this view comes from recent molecular biological results indicating that Oomycota (i.e. benthic, filamentous primitive fungi) are the closest relatives of diatoms (Bhattacharya et al. 1992; Leipe et al. 1994). Because chains with such a morphology have a lower nutrient supply than do solitary cells, this means that nutrient supply in pelagic environments cannot have been the factor that originally led to the evolution of diatom chains. Therefore, either chain formation is a primitive property of diatoms, or, more likely, other factors, possibly related to an originally benthic habitat, must be responsible for the evolution of the first diatom chains.

Large spines also do not increase nutrient supply, but many spines would tend to reduce it. Given some advantage of having long spines (e.g. as a grazing deterrent), this may explain the evolution of chains and cells with very few but very long spines (e.g. in *Chaetoceros* sp.). As chains with gaps can achieve a significantly greater nutrient supply than do compact chains and even solitary cells, nutrient limitation could well explain evolution of spaced chains. Reducing chain length under nutrient limitation, as mentioned above, could also be viewed as a strategy for improving nutrient supply under conditions disadvantageous to chain formation.

## References


BATCHELOR, G. K. 1979. Mass transfer from a particle suspended in fluid with a steady linear ambient velocity distribution. J. Fluid Mech. **95:** 369–400.

BEKLEMISHEV, C. W. 1961. On the role played by the colonies of plankton diatoms. Tr. Inst. Okeanol. **51:** 16–30. (In Russian with English summary.)

BERG, H. C., AND E. M. PURCELL. 1977. Physics of chemoreception. Biophys. J. **20:** 193–219.

BHATTACHARYA, D., AND OTHERS. 1992. Algae containing chlorophylls *a* + *c* are paraphyletic: Molecular evolutionary analysis of the Chromophyta. Evolution **46(6):** 1801–1817.

BOUCHER, D. F., AND G. E. ALVES. 1959. Dimensionless numbers. Chem. Eng. Prog. **55:** 55–64.

CRANK, J. 1975. The mathematics of diffusion, 2nd ed. Clarendon.

DROOP, M. R. 1973. Some thoughts on nutrient limitation in algae. J. Phycol. **9:** 264–272.

FRYXELL, G. A., AND W. I. MILLER III. 1978. Chain-forming diatoms: Three araphid species. Bacillaria **1:** 113–136.

GILLBRICHT, M. 1988. Phytoplankton and nutrients in the Helgoland region. Helgoländer Meeresunters. **42:** 435–467.

HARRISON, P. J., J. S. PARSLOW, AND H. L. CONWAY. 1989. Determination of nutrient uptake kinetic parameters: A comparison of methods. Mar. Ecol. Prog. Ser. **52:** 301–312.

JUMARS, P. A., J. W. DEMING, P. S. HILL, L. KARP-BOSS, P. L. YAGER, AND W. B. DADE. 1993. Physical constraints on marine osmotrophy in an optimal foraging context. Mar. Microb. Food Webs **7:** 121–159.

KARP-BOSS, L., E. BOSS, AND P. JUMARS. 1996. Nutrient fluxes to planktonic osmotrophs in the presence of fluid motion. Oceanogr. Mar. Biol. Annu. Rev. **34:** 71–107.

KIM, S., AND S. J. KARRILA. 1991. Microhydrodynamics: Principles and selected applications. Butterworth.

KIØRBOE, T. 1993. Turbulence, phytoplankton cell size, and the structure of pelagic food webs. Adv. Mar. Biol. **29:** 1–72.

KOEHL, M. A. R., AND J. R. STRICKLER. 1981. Copepod feeding currents: Food capture at low Reynolds number. Limnol. Oceanogr. **26:** 1062–1073.

LAZIER, J. R. N., AND K. H. MANN. 1989. Turbulence and the diffusive layers around small organisms. Deep-Sea Res. **36:** 1721–1733.

LEIPE, D. D., AND OTHERS. 1994. The stramenopiles from a molecular perspective: 16S-like rRNA sequences from *Labyrinthuloides minuta* and *Cafeteria roenbergensis*. Phycologia **33:** 369–377.

LOGAN, B. E., AND A. L. ALLDREDGE. 1989. Potential for increased nutrient uptake by flocculating diatoms. Mar. Biol. **101:** 443–450.

MANN, K. H., AND J. R. N. LAZIER. 1991. Dynamics of marine ecosystems. Blackwell.

MCCARTHY, J. J. 1981. The kinetics of nutrient utilization, p. 211–233. *In* T. Platt [ed.], Physiological bases of phytoplankton ecology. Department of Fisheries and Oceans.

MITCHELL, J. G., A. OKUBO, AND J. A. FUHRMANN. 1985. Microzones surrounding phytoplankton form the basis for a stratified microbial ecosystem. Nature **316:** 58–59.

MONTAGNES, D. J. S., AND J. A. BERGES. 1994. Estimating carbon, nitrogen, protein, and chlorophyll *a* from volume in marine phytoplankton. Limnol. Oceanogr. **39:** 1044–1060.

MOON, P., AND D. E. SPENCER. 1961. Field theory handbook. Springer.

MUNK, W. H., AND G. A. RILEY. 1952. Absorption of nutrients by aquatic plants. J. Mar. Res. **11:** 215–240.

PASCIAK, W. J., AND J. GAVIS. 1974. Transport limitation of nutrient uptake in phytoplankton. Limnol. Oceanogr. **19:** 881–888.

———, AND ———. 1975. Transport limited nutrient uptake rates in *Ditylum brightwellii*. Limnol. Oceanogr. **20:** 604–617.

PRESS, W. H., S. A. TUEKOLSKY, W. T. VETTERLING, AND B. P. FLANNERY. 1992. Numerical recipes in Fortran, 2nd ed. Cambridge Univ.

PURCELL, E. M. 1978. The effect of fluid motions on the absorption of molecules by suspended particles. J. Fluid Mech. **84:** 551–559.

SHIMETA, J., P. JUMARS, AND E. J. LESSARD. 1995. Influences of turbulence on suspension feeding by planktonic protozoa; experiments in laminar shear fields. Limnol. Oceanogr. **40:** 845–859.

SMAYDA, T. J. 1966. Experimental observations on the flotation of marine diatoms. II. *Skeletonema costatum* and *Rhizosolenia setigera*. Limnol. Oceanogr. **11:** 18–34.

———. 1970. The suspension and sinking of phytoplankton in the sea. Oceanogr. Mar. Biol. Annu. Rev. **8:** 353–414.

STRATHMANN, R. R. 1967. Estimating the organic carbon content of phytoplankton from cell volume or plasma volume. Limnol. Oceanogr. **12:** 411–418.

VALIELA, I. 1984. Marine ecological processes. Springer.

WHEELER, P. A., P. M. GLIBERT, AND J. J. MCCARTHY. 1982. Ammonium uptake and incorporation by Chesapeake Bay phytoplankton: Short term uptake kinetics. Limnol. Oceanogr. **27:** 1113–1128.


*Received: 10 July 1996*
*Accepted: 21 April 1997*